2D Metal Organic Framework-Graphitic Carbon Nanocomposites as Precursors for High-Performance O₂-Evolution Electrocatalysts

Tania Rodenas*, Sebastian Beeg, Ioannis Spanos, Sebastian Neugebauer, Frank Girgsdies, Gerardo Algara,-Siller, P. Philipp M. Schleker, Peter Jakes, Norbert Pfänder, Marc Willinger, Mark Greiner, Gonzalo Prieto, Robert Schlögl, and Saskia Heumann*

Dr. T. Rodenas, Dr. S. Beeg, Dr. I. Spanos, Dr. S. Neugebauer, Dr. P. P. M. Schleker, N. Pfänder, Dr. M. Greiner, Prof. R. Schlögl, Dr. S. Heumann
Max-Planck-Institute für Chemische Energiekonversion
Stiftstraβe 34-36, 45470 Mülheim an der Ruhr, Germany
E-mail: tania.rodenas@cec.mpg.de; saskia.heumann@cec.mpg.de

Dr. F. Girgsdies, Dr. G. Algara-Siller, Prof. R. Schlögl
Fritz-Haber-Institut der Max-Planck-Gesellschaft
Faradayweg 4-6, 14195 Berlin, Germany

Dr. P. P. M. Schleker, Dr. P. Jakes
Forschungszentrum Jülich
Wilhelm-Johnen Straβe, 52425 Jülich, Germany

Prof. M. Willinger
Scientific Center for Optical and Electron Microscopy, ETH Zurich
Auguste-Piccard-Hof 1, 8093 Zurich, Switzerland

Dr. G. Prieto
Max-Planck-Institut für Kohlenforschung
Kaiser-Wilhelm-Platz 1, 45470 Mülheim an der Ruhr, Germany

The development of effective and precious-metal-free electrocatalysts for the oxygen evolution reaction (OER) represents a major bottle-neck to unlock a renewable energy scenario based on water splitting technologies. Materials uniting the electrical conductivity of conjugated graphitic nanomaterials with the chemical regularity of metal-organic-framework (MOF) macromolecular crystals are promising precursors for such electrocatalysts. However, a nanoscale integration of these two families of materials represents a challenge. Here we have developed a new synthesis route which integrates 2D metal-organic-framework (MOF) nanocrystals and graphitic carbon nanolamellae into layered heterostructured composites. While the graphitic carrier contributes excellent charge-transport properties, the 2D macromolecular MOF precursor provides a suitable shuttle for introducing highly dispersed metal species into the graphitic matrix, while controlling their direct chemical environment via selection of the organic linker in the parent metal-organic hybrid. Thermal decomposition of 2D cobalt tetrafluoro benzene-dicarboxylate MOF nanocrystals within such composites enables the stabilization of cobalt oxyhydroxyfluoride nanoparticles on the graphitic carrier which display an extraordinary activity for the oxygen evolution reaction in alkaline media, with low onset overpotential (310 mV_{RHE}) and current densities $>10^4$ $mA \cdot cm^{-2} \cdot \mu mol_{Co}^{-1}$ at an operating overpotential of 450 mV, alongside excellent operational stability. In view of the wide compositional array offered by MOFs, this synthesis approach represents a versatile route towards advanced (electro)catalysts and other functional materials for applications from sensing to energy storage and conversion.

1. Introduction

In the quest for widely accessible and efficient water splitting technologies, the development of effective and precious-metal-free electrocatalysts for the oxygen evolution reaction (OER) –a multi-electron half-cell electrochemical reaction with intrinsically sluggish kinetics– currently represents a major barrier.[1] Recently, progress has been achieved in the design and synthesis of OER electrocatalysts based on first-row transition metal active species, with cobalt (oxide)-based materials being a prominent example.[2] For Co-based OER electrocatalysts, experimental[3] and theoretical[4] studies have enabled preliminary structure-performance relationships to be established. The stabilization of high-valence metal centers, e.g. Co(IV), has been proposed to be of critical relevance for the development of active sites under operation conditions.[3a, 5] On this basis, approaches to promote and stabilize such high-valence metal sites through control over the geometry and electronic environment of cobalt cations have been put forward. These strategies involve "self-repairing" cation-anion systems,[6] alloying with electronegative promoters,[7] or tailoring the cobalt coordination sphere in mixed oxides.[3b, 8] In this regard, the use of (macro)molecular metal precursors, with well-defined composition and structure, offers prospects for the assembly of advanced electrocatalysts with high degree of control over the nature and direct chemical environment of the metal species.

At present, metal-organic-frameworks (MOFs) are increasingly drawing interest as macromolecular precursors for metal/carbon functional materials, which can be obtained by controlled thermal decomposition of the pristine crystalline hybrid framework, and show interesting properties in areas spanning from energy storage[9] to adsorption[10] and (electro)catalysis.[11] In electrocatalysis, studies have recently reported the development of MOF-derived electrode materials based on active metal species – originating from the

metallic nodes in the parent MOF – supported on, or embedded within, porous carbon matrices obtained by decomposition of the organic linkers.[12] In contrast to more conventional synthesis methods based on the deposition of metal species on pre-existing carbon carriers by liquid-phase or gas-phase (e.g. chemical vapour deposition) approaches, the structurally and compositionally regular framework of the MOF precursor contributes to a high degree of homogeneity in the composition, size and spatial distribution of the active metal species in the ultimate electrode material.

Unfortunately, *ex*-MOF metal/carbon materials present some major limitations as it comes to their application as electrocatalysts. First, an extra carbon source often needs to be incorporated, prior to decomposition, in order to reduce the overall metal content with respect to that in the MOF precursor and thus avoid excessive metal sintering upon annealing.[13] Second, the decomposition process takes place preserving the shape of the original MOF crystals,[14] typically leading to 3D micrometer-sized, often microporous, structures thus showing sub-optimal mass transport in electrocatalysis. Moreover, the final composites consist of primarily amorphous carbon, with low graphitization degrees, and therefore limited electron conductivity and corrosion resistance. Even though the latter limitation might be overcome by submitting the *ex*-MOF composites to high-temperature graphitization treatments under specific gas atmospheres,[15] a general synthesis strategy uniting the chemical versatility of MOFs, as precursors for carbon-supported metal species, with excellent mass and charge-transport properties is highly sought to develop advanced electrode materials.

Herein we report the synthesis of metal/carbon electrocatalysts via the assembly and decomposition of composite precursors consisting of intercalated two-dimensional (2D) cobalt-based MOF crystals and graphitic lamellae. On the one hand, the compositionally regular MOF crystals represent a suitable shuttle to introduce finely dispersed

4

electrocatalytically active metal species into the graphitic matrix, while controlling their direct chemical vicinity via judicious choice of the organic linker in the starting macromolecular precursor. While highly active OER electrocatalysts based on single 2D nanomaterials such as layered double hydroxides (LDHs)[16] or heteroatom-doped graphene[17] have been described in the recent literature, here we integrate two different 2D nanomaterials into layered composites to showcase nanospatial control over the electrocatalytic promotion effect, bringing a highly electronegative promoter such as fluorine in atomic intimacy with electroactive cobalt species. On the other hand, the graphitic matrix confers remarkable electrical conductivity. The layered morphology of both components in the precursor composite facilitates their integration and improves their mutual contact area thus maintaining a tight contact between the electrically isolating active phase and the highly conductive graphitic current collector in the ultimate electrocatalyst material. This route has been exploited to synthesize noble metal-free electrocatalysts with unprecedented performance for the OER in alkaline media.

2. Results and discussion

Two dimensional cobalt tetrafluoro-benzenedicarboxylate (CoTFBDC) MOF crystals were synthesized following a recently developed bottom-up synthesis method[18] which relies on imposing diffusion control over the MOF crystal growth at the interface between static solutions of the organic linker and metal precursors (experimental details in the methods summary section). Under optimized synthesis conditions, high-quality CoTFBDC MOF nanolamellae were obtained. X-ray diffraction (XRD) confirmed the crystallinity of the MOF material (Figure 1a and Figure S1), while scanning electron microscopy (SEM) imaging revealed an ultrathin crystal morphology, with lateral dimensions predominantly in the sub-μm regime (**Figure 1a**). Separately, lamellae of graphitic carbon were synthesized by liquid-phase exfoliation of high-purity graphite under ultrasonication. The exfoliation process was

monitored with time-resolved Raman spectroscopy, which revealed that a steady exfoliation degree was achieved after 3 hours under the conditions applied (**Figure S2**). High-resolution SEM (**Figure 1b**) and transmission electron microscopy (TEM) characterizations (**Figure S3**) confirmed the successful exfoliation, showing that the product consists predominantly of flakes of few-layer graphitic sheets.
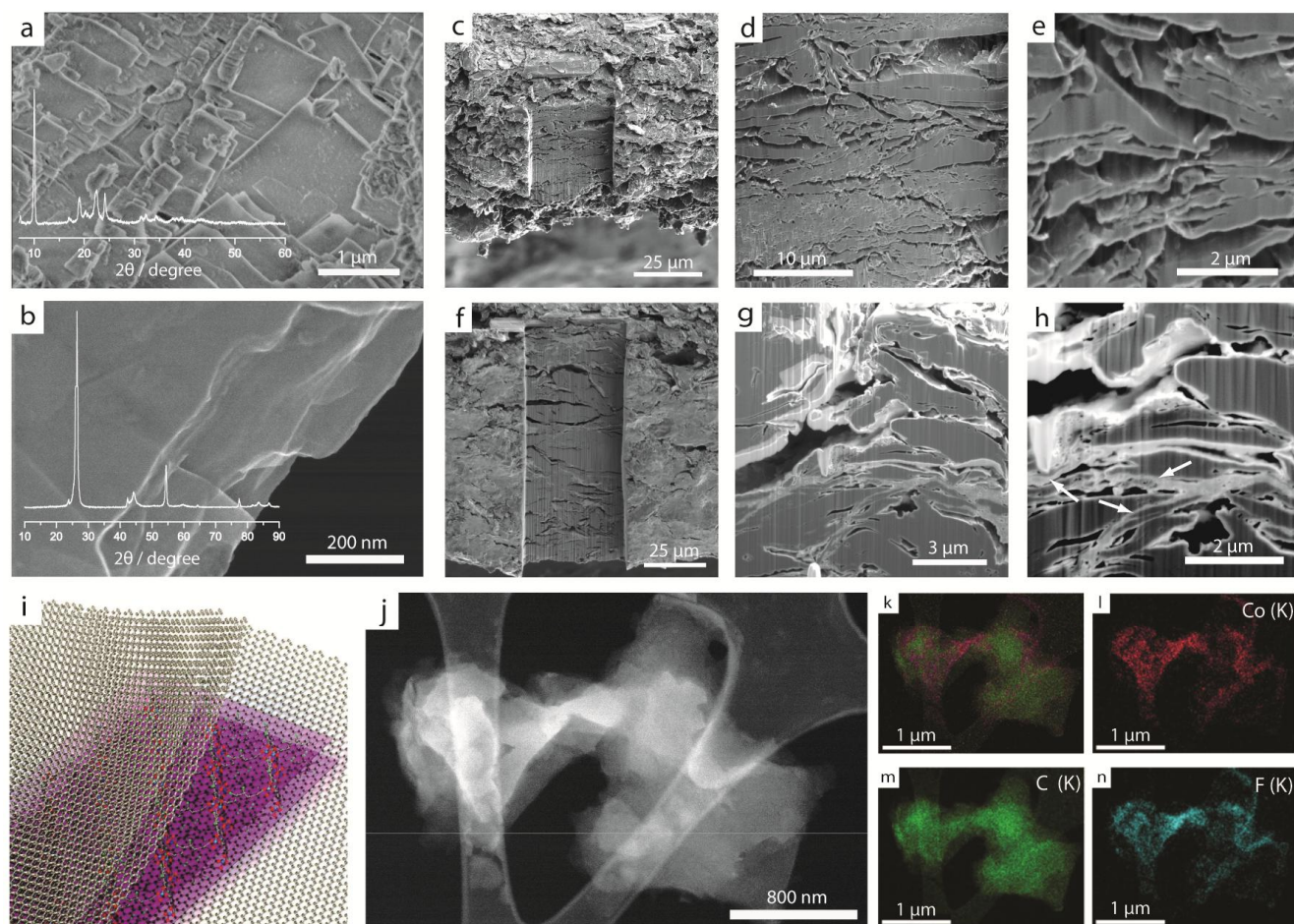

Figure 1. Micro- and nanostructure of MOF nanosheet crystals, exfoliated graphite and composite materials thereof. a) Scanning-electron (SEM) micrograph and X-ray diffractogram (as inset) for the as-prepared CoTFBDC nanosheet crystals. b) SEM micrograph and X-ray diffractogram (as inset) for the as-prepared exfoliated graphite nanosheets. c-e) Cross-sectional SEM micrographs of a consolidated pellet of exfoliated graphite after focused-ion-beam (FIB) milling, and f-h) Cross-sectional SEM micrographs of a CoTFBDC/EG composite (7 wt% Co) after annealing at 250 °C and conformed as a self-supported consolidated pellet after focused-ion-beam (FIB) milling. The MOF nanosheets can be identified within the exfoliated graphite support owing to their higher contrast (brighter objects) and are indicated with arrows in panel h. In all cases, imaging

6

has been performed on FIB-exposed cross-sections oriented perpendicular to the direction mechanical pressure was applied along to conform the pellets. i) Schematic representation of the as-synthesized stacked composite material configuration upon intercalation of nanosheet crystals of the laminar MOF within graphite lamellae. j) HAADF-STEM micrograph of the CoTFBDC/EG composite deposited on a lacey carbon TEM grid. Panels k-n show the EDX spectroscopy elemental maps corresponding to the area imaged in j: k, overlapped elemental maps. l, cobalt. m, carbon. n, fluorine.

MOF and exfoliated graphite (EG) 2D components were integrated to form a heterostructure by co-dispersion in N,N-dimethyl formamide (DMF) followed by slow and complete solvent removal. Fourier-Transform infrared spectroscopy (FTIR) provided evidences for the intercalation of MOF nanocrystals within the EG sheets, which hamper their re-stacking upon drying (**Figure S4**). Moreover, electron paramagnetic resonance (EPR) showed increased electron spin relaxation rates for Co^{2+} ions in the MOF structure upon incorporation into the composites, as a result of an enhanced electron mobility, indicative of an effective electronic contact between the MOF nanocrystals and the conductive EG support material (**Figure S5**). SEM imaging was used on focused-ion-beam (FIB) milled cross-sections of consolidated pellets in order to assess the mesoscale spatial distribution of the two components in the MOF/EG composite materials. As shown in Figure 1f-h, the stacked architecture of the composite was revealed, displaying a highly folded external surface with slit-type pores, for reactant transport, as a result of the stacking of graphite nanosheets. In addition, cross-sectional imaging showed the MOF nanosheet crystals to be uniformly distributed within the pellet at a mesoscopic-micrometer length scale and well integrated with the exfoliated graphite, without obvious gap spaces between the two materials. High-angle annular dark-field scanning transmission electron microscopy (HAADF-STEM) and energy dispersive X-ray spectroscopy (EDX) were applied to investigate the integration of the two materials at the nanoscale. In this case, the mesoscale architecture of the composite was disintegrated by ultrasonication to achieve nanometer thin specimens, thus sufficiently transparent to the

electron beam. As illustrated in Figure 1j-n and **Figure S6**, the resulting MOF/EG composites consist of flakes of EG, with micrometer lateral dimensions, decorated with smaller MOF nanolamellae, identified by their high local concentrations of Co and F. Overall, these results confirmed the successful intercalation of both 2D nanomaterials into an heterostructure, as schematically illustrated in Figure 1i, thus attaining a high contact between the macromolecular metal precursor and the graphitic current collector in the composites.
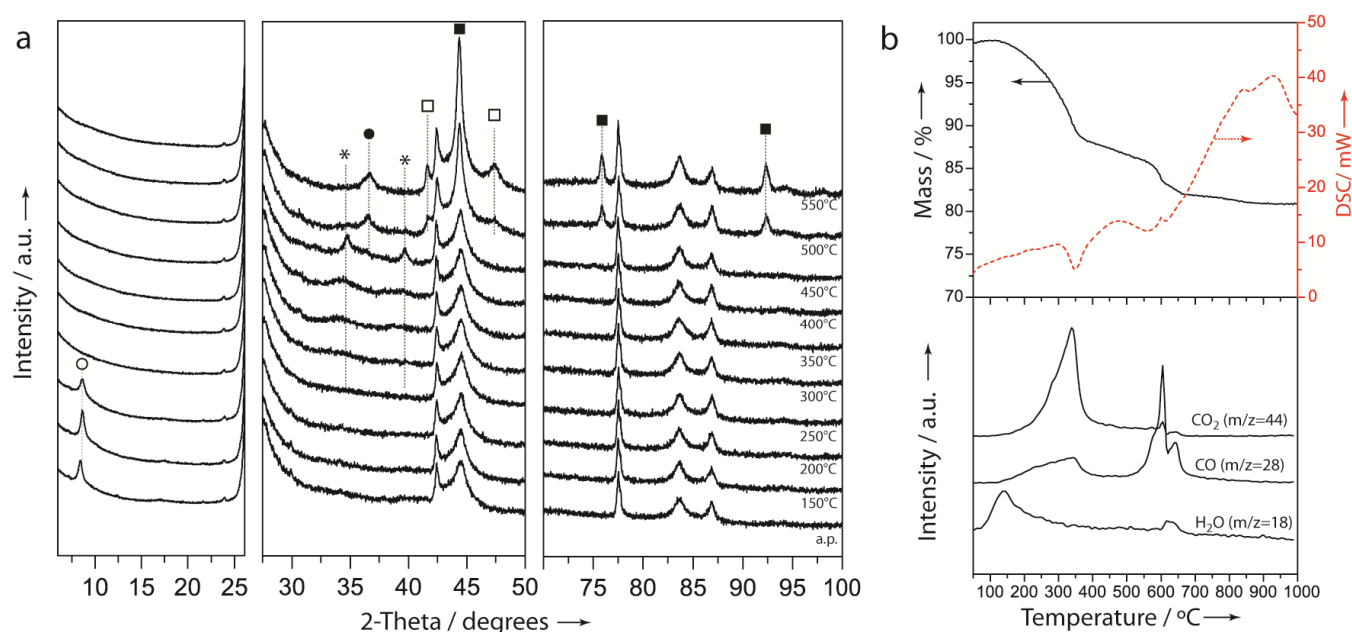
Figure 2. Monitoring of the thermal annealing process for CoTFBDC/EG composite materials. a) Annealing-temperature-resolved X-ray diffractograms for a CoTFBDC/EG composite (7 wt% Co) during its annealing under N_2 atmosphere. Breaks have been introduced in the abscissa axis to enhance visualization of metal diffraction signals over the intense peaks corresponding to the graphitic support. Marked diffraction lines correspond to the CoTFBDC MOF (○), CoF_2, PDF-2 00-033-0417 (*), CoO, PDF-2 03-065-5474 (●), fcc-Co^0, PDF-2 01-089-4307 (■), and hcp-Co^0, PDF-2 01-089-4308 (□). For clarity, diffraction peaks of the graphitic support are not labelled. b) Thermogravimetric and differential scanning calorimetry profiles (top) and corresponding temperature-resolved mass-spectrometry analysis of the evolved gas (bottom) during the decomposition of the CoTFBDC/EG composite under inert Ar flow.

8

Cobalt-based electrocatalyst materials were synthesized by thermal decomposition of the metal-organic-framework precursor in the MOF/EG composites under inert N_2 atmosphere. The annealing process was monitored with XRD and thermogravimetric analysis (TGA), while the nanostructure and (surface) composition of the resulting cobalt species was studied by means of (S)TEM microscopy, Energy Dispersive X-ray (EDX) spectroscopy and X-ray photoelectron spectroscopy (XPS) as a function of the annealing temperature. **Figure 2a** shows the X-ray diffractograms obtained upon treating a CoTFBDC-MOF/EG composite (7 wt% Co) at increasing temperatures up to 550 °C. According to these results, CoTFBDC is stable until about 200-250 °C. At lower temperatures the main diffraction peak of the lamellar MOF shifted progressively to higher angles, indicating the compaction of the individual atomic layers. At higher temperatures (ca. 250 °C), TGA analysis (**Figure 2b**) showed a prominent weight loss (13 %) accompanied by a significant CO_2 release, indicating the decomposition of the dicarboxylic organic linker of the MOF. As a result, very broad X-ray reflections developed, which can be ascribed to CoF_2. The formation of cobalt (II) fluoride as the major crystalline product of MOF decomposition was even more evident on inspection of the XRD patterns, as a function of the annealing temperature, for the unsupported CoTFBDC MOF, for which the metal content is higher (**Figure S7**). TEM analysis of the composite annealed at 250 °C (CoTFBDC/EG_250) showed the decomposition of the EG-supported 2D MOF crystals into flakes consisting of metal nanocrystallites (1 to 5 nm in size) embedded within a framework of amorphous-carbon (**Figure 3a-d**). The carbon matrix around the metal nanocrystals originates from the decomposition of the dicarboxylate linker of the MOF and was found to be mainly microporous by N_2-physisorption (**Figure S8**). A lattice spacing of 0.33 nm was determined for the embedded nanocrystals (**Figure 3d**), in agreement with the *d*-value expected for the prevalent (110) plane of CoF_2 (PDF-2 00-033-0417). Few larger cobalt oxide crystals (up to 100 nm) were also observed, rather disconnected from the carbon support material (**Figure S9**) which originate, likely, from the decomposition of residues of

the cobalt precursor employed in the MOF synthesis and retained after washing. These larger crystals could not be detected by XRD, indicating that they account only for a minor fraction of the metal in the activated composite. Jointly, these results show that thermal decomposition of the EG-supported 2D MOF crystals results in the chemical association of cobalt and fluorine species and the stabilization of the resulting metal fluoride nanocrystals within a MOF-derived carbon matrix in close contact with the graphitic carrier.

Increasing the annealing temperature in the range of 250 °C-500 °C led first to a progressive sharpening, followed by disappearance of the CoF_2 diffraction lines, indicating crystal growth and decomposition, respectively. New diffraction peaks for CoO and metallic Co^0, predominantly fcc, set in at 500 °C, which narrowed and gained intensity on further increasing the temperature to 550 °C. It is hence inferred that annealing temperatures above 250 °C first induce the segregation of cobalt and fluorine species and metal reduction, to which a significant metal particle growth follows. This is indeed clearly shown by (S)TEM/EDX inspection of the material obtained by annealing at 550 °C (**Figure 3e-h and Figure S10**), which showed metallic Co nanoparticles, in a broad size range, from ca. 3 up to >100 nm, with an oxide outerlayer. These metal particles are no longer embedded within an amorphous carbon matrix (**Figure S10g**). This observation is in agreement with the TGA analysis (**Figure 2b**), which showed a second prominent weight loss (5 %) at ca. 550 °C, accompanied by the release of CO, confirming the gasification of the MOF-derived amorphous carbon around the metal species, likely catalyzed by the nascent Co^0 crystals. The disappearance of the protective carbon matrix facilitates the extensive metal agglomeration observed at these higher annealing temperatures.

X-ray photoelectron spectroscopy (XPS) was used to assess the near-surface composition and speciation of Co and F species as a function of the annealing temperature (**Figure 3i**). After drying at 150 °C, a near-surface F/Co atomic ratio of 2.89 was determined, which is lower

10

than the experimental bulk ratio (4.48, **Table S1**) and that expected from the stoichiometry of

the MOF structure (4.00), indicating a certain surface enrichment in cobalt. For this material,

a Co2p binding energy (BE) of 783.9 eV and the detection of the characteristic shake-up

satellite features agree with the existence of Co^{2+}-carboxylates in the structure of the

CoTFBDC coordination polymer. The corresponding F1s spectrum showed a major

component at a BE of 690.2 eV, which was also the only F1s band detected for the

corresponding unsupported CoTFBDC MOF (peaking at 690.1 eV, **Figure S11**). This BE is

characteristic of polyfluorinated benzene rings[19] and can thus be ascribed to the fluorinated

organic linker in the MOF structure. Next to this major component, two lower BE

contributions were additionally detected in the composite. The band at 689.1 eV falls in the

range of electron-rich covalent C-F species and can thus arise from an electronic interaction

of a fraction of the fluorinated linkers in the 2D MOF crystals with the electron-donating

graphitic support. The second contribution peaking at 687.8 eV has been reported for

fluorinated graphene[20] and suggests that, already at mild temperatures (150 ºC), part of the

fluorine is emitted from the MOF, migrates by spillover and reacts with the graphitic support.

The O1s spectrum could be deconvoluted into two components. The major one at 534.4 eV

was detected as a single contribution in the unsupported MOF (Figure S10) and is thus

ascribed to the carboxylate moieties in the linker. The lower BE contribution at 532.1 eV

arises from oxygen groups on the graphitic carrier.[21]
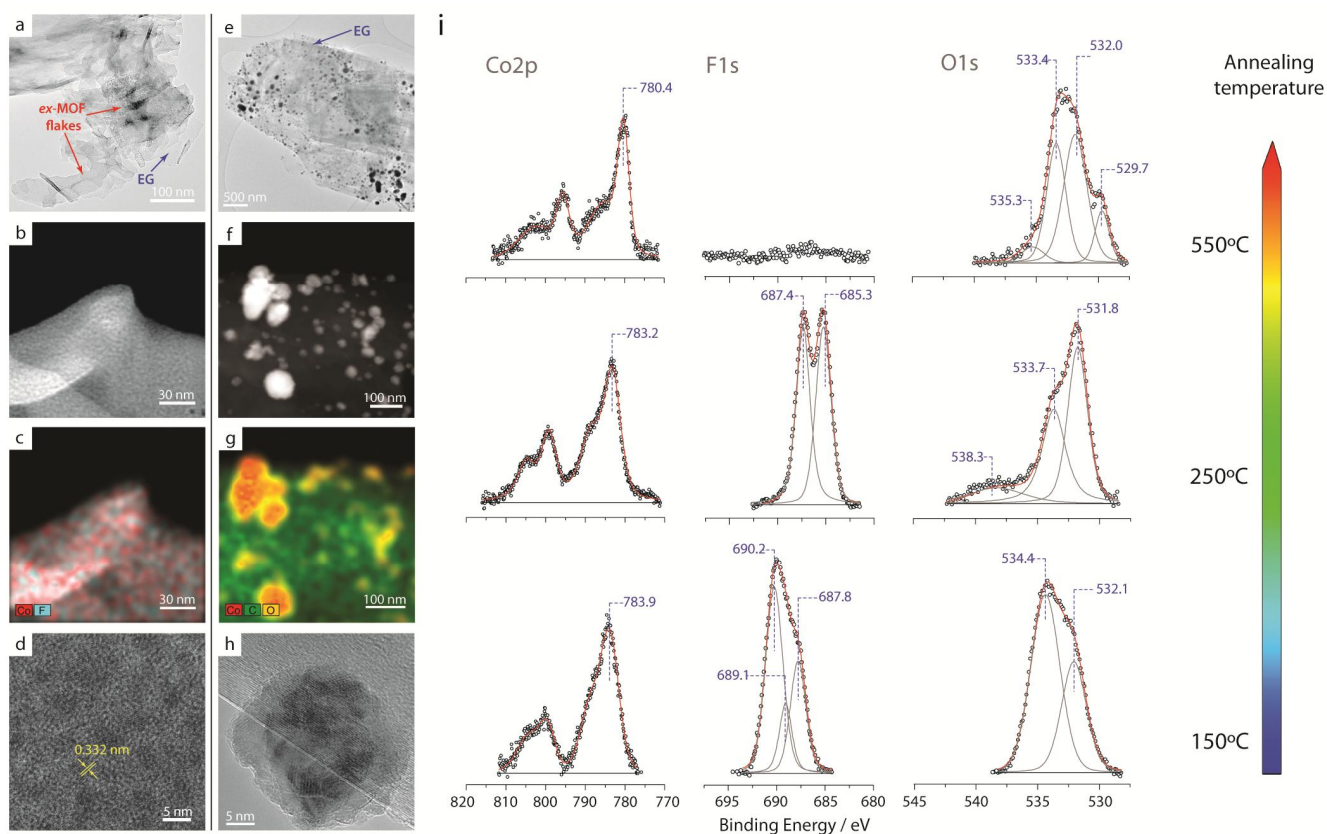
Figure 3. Temperature-resolved size and near-surface speciation of metal species in CoTFBDC/EG composite materials. a-h) Nanoscale imaging and spectroscopy of the CoTFBDC/EG composite; a,e) bright-field TEM micrographs; b,f) HAADF-STEM micrographs; c,g) EDX elemental mapping; d,h) high-resolution TEM micrographs for the electrocatalysts obtained upon annealing a CoTFBDC/EG composite (7 wt% Co) at 250 °C (panels a-d) and 550 °C (panels e-h) in N_2 flow. i) X-ray photoelectron spectra (Co2p, F1s and O1s spectral regions) after annealing the CoTFBDC/EG composite at 150 ℃, 250 °C and 550 °C in N_2 flow.

After annealing at 250 °C, both the bulk and near-surface F/Co atomic ratio have decreased by about 35% (**Table S1**), indicating the loss of a fraction of the fluorine as a volatile species. The Co2p BE of 783.2 eV is fully consistent the formation of cobalt CoF_2 upon decomposition of the MOF precursor.[22] This interpretation is fully in line with the XRD results and is indeed reinforced upon analysis of the F1s photoemission spectra. All fluorine species with BE>689 eV have vanished upon reaching an annealing temperature of 250 °C, confirming the quantitative decomposition of the organic linker in the MOF precursor. Two equivalent F1s contributions peaking at 687.4 and 685.3 eV are detected instead, which can be

ascribed to fluorine covalently bonded to carbon and ionic-type fluorine species in CoF_2, respectively.[22] It is therefore inferred that, following the thermal decomposition of the MOF, only approximately half of the fluorine existing on the surface of the material has reacted with Co^{2+}, the rest remaining covalently associated to carbon species, either those originating from the MOF decomposition or the graphitic carrier. This result is consistent with the fact that the nominal F/Co atomic ratio in the pristine MOF (4.00) doubles the stoichiometric fluorine content required for the formation of CoF_2. The corresponding O1s spectrum confirms the decomposition of the carboxylated MOF linkers, while the remaining surface oxygen corresponds to functional groups on the carbon support. Further increasing the annealing temperature to 550 °C leads to a significant shift in the Co2p band to a lower BE of 780.4 eV. This shift indicates an increased covalence in the coordination of the Co^{2+}, and is consistent with the predominance of CoO on the outer surface, in agreement with the nanometer thick oxide overlayer detected on metallic Co^0 particles by HR-(S)TEM. No significant surface metallic cobalt contribution could be detected by XPS, suggesting the complete passivation of the metallic particles by an oxide overlay. The surface Co/C atomic ratio (**Table S1**) decreases ca. fivefold upon increasing the annealing temperature from 250 °C to 550 °C, in spite of the (partial) gasification of MOF-derived carbon ascertained by TGA-MS (**Figure 2b**), which agrees with the considerable metal sintering observed by (S)TEM. At this temperature, both near-surface XPS and bulk-type EDX analyses evidenced that the fluorine concentration is below the detection limits of the respective methods (**Table S1**), demonstrating that fluorine not only segregates from cobalt but also quantitatively leaves the material as a volatile species at sufficiently high annealing temperatures. Overall, the results reveal a dual role of the fluorine introduced as part of the organic linker in the 2D MOF precursor. On the one hand, it leads to the formation of nanosized CoF_2 crystals embedded within a MOF-derived amorphous carbon matrix at the temperature of incipient MOF decomposition (250 ºC). On the other hand, the surplus of fluorine migrates by spillover and functionalizes the

13

carbon carrier, an effect which is expected to have positive electrocatalytic effects, such as healing oxidation sites, thus enhancing stability against corrosion, and increasing hydrophobicity, hence contributing to an efficient release of O_2 bubbles from the surface of the working electrocatalyst.[23]

The OER electrocatalytic activity of the MOF/EG composites and their annealing products was assessed in alkaline media following a standardized protocol.[23] The main electrocatalysis results are summarized in **Figure 4**. First, the electrocatalysts were activated by cyclic voltammetry (CV) in the potential range of 0.84-1.45 V (vs. RHE) at a rate of 100 mV·s^{-1}. Very stable CV traces were registered for 50 cycles, indicating a significant resistance of the electrocatalysts to corrosion. Preliminary electrocatalysis tests run with comparative materials obtained by decomposition of a fluorine-free CoBDC/EG composite (**Figure S12**) confirmed the key role of the fluorine-functionalized organic linker in the MOF precursor to obtain the most active electrocatalysts (**Figure S13**).

Not only the presence of fluorine in the starting composite, but also its chemical association with cobalt species was found to be determinant for the electrocatalytic performance. **Figure 4a** depicts the CV traces obtained for various electrocatalysts derived from a CoTFBDC-MOF/EG composite with a 7 wt% Co loading. The shape of the CV loops is in all cases typical for cobalt-based electrocatalysts. An anodic peak detected at ca. 1.15 V_{RHE} can be assigned to the Co(II)/Co(III or IV) redox process, which is generally believed to be responsible for the formation of high-valence cobalt species as the (most) active OER sites.[24] Compared to the as-synthesized composite, or materials obtained by annealing at alternative temperatures, CoTFBDC/EG_250 – annealed at 250 °C, which corresponds to the minimum temperature required for MOF decomposition – showed the highest specific capacitance along with the lowest potential for the cathodic reduction peak (ca. 1.12 V_{RHE}). The superior performance of this electrocatalyst was also determined by stationary polarization (SP)

14

measurements. **Figure 4b** depicts the SP curves for the series of MOF/EG composite-derived electrocatalysts along with a benchmark cobalt oxide-based electrocatalyst prepared according to literature procedures.[25] Low onset overpotentials in the range of 310-368 mV were registered for the entire set of composite-derived electrocatalysts. **Figure 4c** shows the metal-specific OER activity at two preset bias voltage values, i.e. 1.6 and 1.8 V corresponding to overpotentials of 365 and 450 mV, respectively (after correction for the electrolyte resistance) as a function of the composite annealing activation temperature. A volcano trend is observed regardless of the selected bias level. The activity registered for the MOF/EG composite as-prepared and treated at a low temperature of 150 °C is very similar, and thus in agreement with the persistence of the parent MOF as the source of active sites in both materials. However, the OER activity increased dramatically after annealing at 250 °C, reaching a metal-specific current density of $11 \cdot 10^3$ mA·cm^{-2}·µmol$_{Co}^{-1}$ at a bias potential of 1.8 V$_{RHE}$, much higher than that registered for Co(Ni) oxide benchmark electrocatalysts at the same potential. The activity decreased again for materials obtained at increasingly higher annealing temperatures in the range of 350 °C-550 °C. The optimal OER activity achieved after annealing at the temperature of incipient MOF decomposition ranks CoTFBDC/EG_250, to our knowledge, among the most active, if not the most, reported cobalt OER electrocatalyst in alkaline media (**Table S2**).
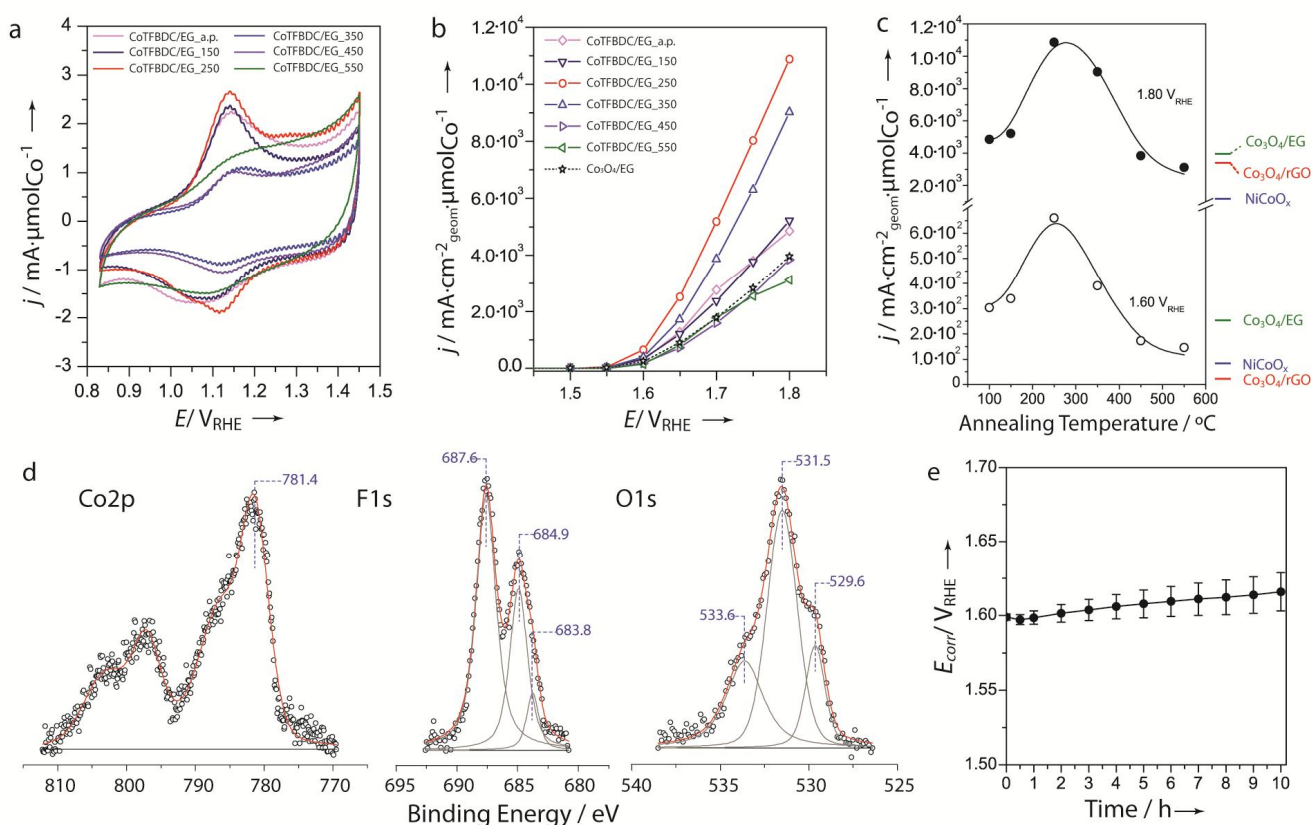
Figure 4. Electrocatalytic evaluation of CoMOF/EG composite-derived catalysts in the oxygen evolution reaction (OER). a) Cyclic voltammetry curves. b) Stationary polarization curves. c) Evolution of the metal-specific current density, determined in the stationary polarization experiments at two selected bias voltage levels of 1.60 V_{RHE} and 1.80 V_{RHE}, respectively, with the annealing temperature for a CoTFBDC/EG composite (7 wt%Co). For reference purposes, the current densities (also normalized per unit metal content) obtained with a commercial $NiCoO_x$, and reference Co_3O_4/rGO and Co_3O_4/EG catalysts prepared according to literature procedures are also shown. d) XPS spectra for the CoTFBDC/EG_250 electrocatalyst after OER action. e) Stability test: evolution of the corrected working potential required to maintain a constant specific current density of 10 $mA·cm^{-2}$ over a total operation period of 10 hours with CoTFBDC/EG_250. Error bars correspond to the standard deviation from three independent runs.

Further evidence of the extraordinary catalytic activity of CoTFBDC/EG_250 were provided by a Tafel-plot analysis (**Figure S14**) which revealed the lowest Tafel slope of 39.8 $mV·dec^{-1}$ for this material. Such Tafel slope is among the lowest reported in the literature for non-noble metal-based OER electrocatalysts, indicative of excellent reaction kinetics. Also for this

16

catalyst was the highest double-layer capacitance (C_{dl}) of 4.68 mF·cm^{-2} determined, i.e. more than six-fold higher than for the comparative electrocatalyst derived from a F-free CoBDC/EG composite material activated at the corresponding optimal (incipient MOF decomposition) annealing temperature (350 °C in this case) (**Figure S15**). These results support the key role of the fluorine promotion to achieve optimal electron transfer between the electrochemically active metal surface and the electrolyte, responsible for the outstanding OER activity. Such synergistic promotion, achieved through the adjustment of the direct chemical environment of the cobalt species via selection of the linker composition in the parent MOF structure, is lost at higher annealing temperatures, which promote the segregation of Co and F. Indeed, the SP curves approach an activity representative of (EG-supported) cobalt oxides – employed as benchmarks in this study – as the annealing temperature increases from the optimal 250 °C to 550 °C, at which temperature the majority of the metal species exist as Co^0 nanocrystals with an outer CoO_x layer. Jointly, physicochemical characterization and electrocatalysis results point to a strong correspondence between OER activity and the speciation of the metal species in the catalysts, which are in turn determined by the final annealing temperature. The highest activity corresponds to the prevalence of cobalt fluoride nanocrystals, which develop upon (incipient) decomposition of the EG-supported MOF nanocrystals, in the activated electrocatalyst.

XPS was applied as a means to gain insight into the nature of the surface active species in the working electrocatalyst. The optimal CoTFBDC/EG_250 electrocatalyst was developed by thermal annealing of the pristine composite on a gold-based carrier. This substrate can play the dual role of electrode and XPS sample holder, thus enabling the XPS characterization of the very same catalyst aliquot both prior to and after electrocatalysis (see Experimental details in the Supporting Information). **Figure 4d** shows the XPS spectra recorded for the material after its electrocatalytic action. For the Co2p signal, a notably low BE of 781.4 eV suggests

the formation of surface cobalt (II) hydroxyfluoride ($CoF_x(OH)_y$) species under OER conditions.[26] This assignment is reinforced by the down-shift in BE observed in the F1s signal for ionic fluorine from 685.3 eV (before electrocatalysis, Figure 3i) to 684.9 eV (after electrocatalysis, **Figure 4d**), the latter BE being consistent with hydroxyfluoride species.[26] It hence stands to reason that these species, which develop on the surface of the working electrode, are the actual electroactive species. After the electrocatalysis test, intensity of the band for ionic F^- species has decreased slightly with respect to that ascribed to the covalent fluorine functionalization of the carbon support (BE=687.6 eV). This observation would agree with the facts that the fluorinated carbonaceous species existing on the surface of the materials are stable under OER conditions, while the *in situ* development of $CoF_x(OH)_y$, by hydroxylation of the pristine CoF_2 nanocrystals, involves the emission of a fraction of the outer-surface fluorine. Indeed, the observation of a third, minor F1s contribution at an even lower BE of 683.8 eV after electrocatalysis can be ascribed to the precipitation of small amounts of KF by reaction of the released F^- anions with K^+ cations from the electrolyte. After this initial activation, the electrocatalyst showed a remarkable stability. Under standard working conditions, a minor cumulative increase of 1% in the overpotential was required to maintain a current density of 10 mA·cm^{-2} over a total operation period of 10 hours (**Figure 4e**). Moreover, no cobalt leaching was observed by *operando* monitoring of the liquid electrolyte with online inductively coupled plasma-optical emission spectroscopy (ICP-OES) in a flow-cell system,[27] unlike for comparative catalysts having either the pristine MOF or CoO_x species as the source of active sites, which showed measurable metal dissolution, particularly during the first 30 minutes of operation (**Figure S16**). Jointly, the results strongly suggest the development of $CoF_x(OH)_y$ species by surface hydroxylation of the *ex*-MOF CoF_2 nanocrystals which are stable under OER conditions, and are therefore responsible for the extraordinary electrocatalytic activity displayed by the composite after optimal annealing activation. These species, in which Co^{2+} cations exist in a highly electronegative chemical

environment, had been proposed as highly active OER catalysts.[26] However, their synthesis as nanosized supported species had remained as an elusive challenge. The herein presented synthesis route provides a pathway for their development as very small nanocrystals in direct association to lamellar graphitic supports, resulting in exceptionally active OER electrocataysts in alkaline media.

Conclusion

In summary, novel layered heterostructured composite materials have been synthesized by integration of ultrathin (2D) cobalt MOF nanocrystals and graphitic nanosheets. As precursors for high-performance and noble-metal-free electrocatalysts, the composites unite the charge-transport properties of the graphitic component with the suitability of the 2D macromolecular MOF precursor as a shuttle to introduce highly dispersed metal species while adjusting their direct chemical environment. For composites incorporating a cobalt MOF with fluorinated organic linkers, activation by annealing at mild temperatures – corresponding to the incipient MOF decomposition – enables the stabilization of very small CoF_2 nanocrystals on the graphitic support, which under electrocatalysis conditions are readily hydroxylated into $CoF_x(OH)_y$ species. The nanosized fluorinated cobalt species display the highest specific OER activities to our knowledge reported thus far for cobalt-based catalysts, alongside remarkable stability in alkaline media. We ascribe this significant performance to the highly electron-withdrawing chemical environment of cobalt cations in the hydroxyl-fluorinated active species. Beyond these findings, it is expected that further structural optimization of parameters such as MOF crystal thickness and lateral size, as well as the stacking degree of the EG carrier, can lead to further improvements in performance. Moreover, in view of the large compositional options offered by metal-organic-frameworks, we envisage our synthesis approach as a versatile route towards advanced electrocatalysts and other functional materials for various other applications such as energy storage or catalysis, where control over the

direct chemical environment of highly dispersed carbon-supported metal species might be highly beneficial.

Experimental section

Synthesis of CoTFBDC nanosheets MOF crystals

Cobalt tetrafluorobenzenedicarboxylate CoTFBDC MOF nanosheet crystals were synthesized in a glass test tube following a bottom-up synthesis strategy published previously.[18] A solution of the organic linker precursor, composed of 0.10 mmol of tetrafluoroterephthalic acid (H_2TFBDC) dissolved in a mixture of 2 mL DMF and 1 mL CH_3CN, was poured into the bottom of the tube. Over this solution, a mixture of 1 mL DMF and 1 mL CH_3CN was added in the role of an intermediate solvent layer to initially separate the solutions of the organic and metal MOF nutrients. Finally, a metal precursor solution, composed of 0.10 mmol $Co(AcO)_2 \cdot 4H_2O$ dissolved in a mixture of 1 mL DMF and 2 mL CH_3CN, was added to the tube as the top layer. The synthesis proceeded at $0 – 2$ °C for 24 h under static conditions, and the resulting precipitate was collected by centrifugation and washed consecutively three times with DMF (3 mL each step) followed by another three times with $CHCl_3$ (3 mL each step). The resulting material was left suspended in $CHCl_3$ until the synthesis of the composite materials. Under these synthesis conditions, a 48 % MOF yield was obtained.

Synthesis of exfoliated graphite (EG) nanosheets

Graphite was added to N,N-dimethyl formamide (DMF) to achieve a concentration of 0.75 mg·mL^{-1}, and then the mixture was treated in an ultrasonication bath (Sonorex Super RK 510, power=400 W, frequency=35 kHz) for 3 hours. To prevent overheating, the water in the sonication bath was maintained at a temperature lower than 30 °C. The resulting suspension was centrifuged at 5000 rpm for 10 min to remove non-exfoliated graphite agglomerates. The supernatant was a stable suspension, which was recovered for further use in the synthesis of the MOF/EG composites.

Synthesis of MOF/exfoliated graphite composites (MOF/EG)

To synthesize the MOF/EG composite materials, freshly-prepared suspensions of the Co-MOF nanosheet crystals and exfoliated-graphite in DMF were mixed in a ratio determined by the nominal cobalt loading set for the final composite. The resulting suspension was magnetically stirred for 1 h (800 rpm) at room temperature and the solvent was then evaporated at reduced pressure in rotatory evaporator at 90 °C. The solid recovered was further dried overnight at 100 °C in a vacuum oven. Next, a series of electrocataly26sts was obtained from a single as-prepared composite by thermal annealing in a tubular oven at various temperatures (150 °C-550 °C) under a flow of N_2 (15 mL·min^{-1}). A heating rate of 2.5 °C·min-1 was employed to the final annealing temperature, followed by a dwell period of 2 h. Scheme S1 illustrates the synthesis of MOF/EG composite materials and their thermal decomposition into the final electrocatalysts.

MANGAN standard electrocatalytic testing procedure

The eletrocatalytic properties of the synthesized materials were determined for the oxygen evolution reaction (OER) in an air-saturated alkaline (1M KOH) solution at a constant temperature of 25 °C, controlled by a cryostat (Lauda Compact Thermostats RCS 20-D). We have applied a rotating electrode standardized protocol established in the framework of the MANGAN project, a German cluster research consortium funded by the German Ministry of Research and Education (BMBF) which, among other objectives, develops generic methods for comparison of electrocatalytic results across 26 research groups. The complete procedure is summarized in Scheme S2, while an example of the results obtained for a selected electrocatalyst is summarized in **Figure S17**. Electrochemical measurements were carried out in a compact and modular potentiostat/galvanostat Metrohm Autolab PGSTAT 204 device run on the NOVA software and equipped with an impedance module jacketed glass-free electrochemical 3-electrode half-cell reactor. A Hg/HgO electrode and Pt wire were used as a

reference electrode (RE) and a counter electrode (CE), respectively. The working electrode (WE) was a rotating disk electrode (RDE) consisting of a glassy carbon disk electrode (4 mm diameter) in a polyether ether ketone (PEEK) sheath.

In all cases, potentials were converted with reference to the Reversible Hydrogen Electrode (RHE) scale according to the Nernst equation (Equation 1):

$$E_{RHE} = E_{Hg/HgO} + 0.059 \text{ x pH} + 0.098 \qquad \text{(Equation 1)}$$

Further details on the experimental methods can be found in the Supplementary Information.

Acknowledgements

Author contributions

T.R. conceived the research, carried out material synthesis and basic characterization and performed the electrocatalytic tests. S.B. and M.G. performed XPS characterization. I.S. contributed the operando ICP-OES study. S.N. developed the electrocatalysis setup and data analysis protocol. F.G. contributed the XRD characterization. G.A.-S., N.P. and M.W.

contributed the (S)TEM and EDX characterizations. P.P.M.S. and P.J. contributed the EPR characterization. G.P. contributed to the conception of the study as well as FIB-SEM, physisorption and EDX characterizations. R.S. and S.H. supervised the study. T.R. wrote the manuscript with input from G.P. S.H. and R.S. All authors contributed to data analysis and manuscript revision.

References

[1]   a) R. Schlogl, *Chemsuschem* 2010, *3*, 209-222; b) E. Fabbri, A. Habereder, K. Waltar, R. Kotz, T. J. Schmidt, *Catal Sci Technol* 2014, *4*, 3800-3821; c) N. T. Suen, S. F. Hung, Q. Quan, N. Zhang, Y. J. Xu, H. M. Chen, *Chem Soc Rev* 2017, *46*, 337-365.

[2]   X. H. Deng, H. Tuysuz, *Acs Catal* 2014, *4*, 3701-3714.

[3]   a) C. N. Brodsky, R. G. Hadt, D. Hayes, B. J. Reinhart, N. Li, L. X. Chen, D. G. Nocera, *P Natl Acad Sci USA* 2017, *114*, 3855-3860; b) R. G. Hadt, D. Hayes, C. N. Brodsky, A. M. Ullmann, D. M. Casa, M. H. Upton, D. G. Nocera, L. X. Chen, *J Am Chem Soc* 2016, *138*, 11017-11030.

[4]   a) I. C. Man, H. Y. Su, F. Calle-Vallejo, H. A. Hansen, J. I. Martinez, N. G. Inoglu, J. Kitchin, T. F. Jaramillo, J. K. Norskov, J. Rossmeisl, *Chemcatchem* 2011, *3*, 1159-1165; b) V. Stamenkovic, B. S. Mun, K. J. J. Mayrhofer, P. N. Ross, N. M. Markovic, J. Rossmeisl, J. Greeley, J. K. Norskov, *Angew Chem Int Edit* 2006, *45*, 2897-2901.

[5]   J. G. McAlpin, Y. Surendranath, M. Dinca, T. A. Stich, S. A. Stoian, W. H. Casey, D. G. Nocera, R. D. Britt, *J Am Chem Soc* 2010, *132*, 6882-6883.

[6]   D. A. Lutterman, Y. Surendranath, D. G. Nocera, *J Am Chem Soc* 2009, *131*, 3838-3839.

[7]   B. S. Yeo, A. T. Bell, *J Am Chem Soc* 2011, *133*, 5587-5593.

[8]   J. Suntivich, K. J. May, H. A. Gasteiger, J. B. Goodenough, Y. Shao-Horn, *Science* 2011, *334*, 1383-1385.

[9]   W. Xia, A. Mahmood, R. Q. Zou, Q. Xu, *Energ Environ Sci* 2015, *8*, 1837-1866.

[10]   J. Wang, J. F. Yang, R. Krishna, T. Yang, S. G. Deng, *J Mater Chem A* 2016, *4*, 19095-19106.

[11]   a) B. Y. Guan, L. Yu, X. W. Lou, *Energ Environ Sci* 2016, *9*, 3092-3096; b) V. P. Santos, T. A. Wezendonk, J. J. D. Jaen, A. I. Dugulan, M. A. Nasalevich, H. U. Islam, A. Chojecki, S. Sartipi, X. Sun, A. A. Hakeem, A. C. J. Koeken, M. Ruitenbeek, T. Davidian, G. R. Meima, G. Sankar, F. Kapteijn, M. Makkee, J. Gascon, *Nat Commun* 2015, *6*.

[12]   a) A. Mahmood, W. H. Guo, H. Tabassum, R. Q. Zou, *Adv Energy Mater* 2016, *6*; b) C. J. Xuan, J. E. Wang, J. Zhu, D. L. Wang, *Acta Phys-Chim Sin* 2017, *33*, 149-164.

[13]   W. Chaikittisilp, K. Ariga, Y. Yamauchi, *J Mater Chem A* 2013, *1*, 14-19.

[14]   B. Y. Xia, Y. Yan, N. Li, H. B. Wu, X. W. Lou, X. Wang, *Nat Energy* 2016, *1*.

[15]   A. Aijaz, J. Masa, C. Rosler, W. Xia, P. Weide, A. J. R. Botz, R. A. Fischer, W. Schuhmann, M. Muhler, *Angew Chem Int Edit* 2016, *55*, 4087-4091.

[16]   a) Y. Y. Wang, C. Xie, Z. Y. Zhang, D. D. Liu, R. Chen, S. Y. Wang, *Adv Funct Mater* 2018, *28*; b) P. Zhou, Y. Y. Wang, C. Xie, C. Chen, H. W. Liu, R. Chen, J. Huo, S. Y. Wang, *Chem Commun* 2017, *53*, 11778-11781.

[17]   a) S. Chen, J. J. Duan, J. R. Ran, M. Jaroniec, S. Z. Qiao, *Energ Environ Sci* 2013, *6*, 3693-3699; b) R. Li, Z. D. Wei, X. L. Gou, *Acs Catal* 2015, *5*, 4133-4142.

[18]   T. Rodenas, I. Luz, G. Prieto, B. Seoane, H. Miro, A. Corma, F. Kapteijn, F. X. L. I. Xamena, J. Gascon, *Nat Mater* 2015, *14*, 48-55.

[19]   D. T. Clark, D. Kilcast, D. B. Adams, W. K. R. Musgrave, *Journal of Electron Spectroscopy and Related Phenomena* 1972, *1*, 227-250.

[20]   Y. Wang, W. C. Lee, K. K. Manga, P. K. Ang, J. Lu, Y. P. Liu, C. T. Lim, K. P. Loh, *Adv Mater* 2012, *24*, 4285-4290.

[21]   R. A. Quinlan, Y. C. Lu, D. Kwabi, Y. Shao-Horn, A. N. Mansour, *J Electrochem Soc* 2016, *163*, A300-A308.

[22]   J. L. Tan, L. Liu, S. P. Guo, H. Hu, Z. C. Yan, Q. Zhou, Z. F. Huang, H. B. Shu, X. K. Yang, X. Y. Wang, *Electrochim Acta* 2015, *168*, 225-233.

[23]   A. Tressaud, E. Durand, C. Labrugere, A. P. Kharitonov, L. N. Kharitonova, *J Fluorine Chem* 2007, *128*, 378-391.

[24]   M. Risch, F. Ringleb, M. Kohlhoff, P. Bogdanoff, P. Chernev, I. Zaharieva, H. Dau, *Energ Environ Sci* 2015, *8*, 661-674.

[25]   Y. Y. Liang, Y. G. Li, H. L. Wang, J. G. Zhou, J. Wang, T. Regier, H. J. Dai, *Nat Mater* 2011, *10*, 780-786.

[26]   S. Wan, J. Qi, W. Zhang, W. Wang, S. Zhang, K. Liu, H. Zheng, J. Sun, S. Wang, R. Cao, *Adv Mater* 2017, *29*.

[27]   I. Spanos, A. A. Auer, S. Neugebauer, X. Deng, H. Tüysüz, R. Schlögl, *Acs Catal* 2017, *7*, 3768-3778.